applied sciences

MDPI

Article

Terahertz Time-Domain Spectroscopy of Graphene Nanoflakes Embedded in Polymer Matrix

Anton Koroliov [1,†], Genyu Chen [2], Kenneth M. Goodfellow [3], A. Nick Vamivakas [3], Zygmunt Staniszewski [4], Peter Sobolewski [4], Mirosława El Fray [4,*], Adam Łaszcz [5], Andrzej Czerwinski [5], Christiaan P. Richter [6] and Roman Sobolewski [1,2,5,*]

1 Department of Electrical and Computer Engineering and the Laboratory for Laser Energetics, University of Rochester, Rochester, NY 14627-0231, USA; anton.koroliov@ftmc.lt
2 Materials Science Program and the Laboratory for Laser Energetics, University of Rochester, Rochester, NY 14627, USA; gchen21@ur.rochester.edu
3 The Institute of Optics, University of Rochester, Rochester, NY 14627, USA; kgoodfel@ur.rochester.edu (K.M.G.); nick.vamivakas@rochester.edu (A.N.V.)
4 Polymer Institute, West Pomeranian University of Technology, PL-70322 Szczecin, Poland; zstaniszewski@zut.edu.pl (Z.S.); psobolewski@zut.edu.pl (P.S.)
5 Institute of Electron Technology, PL-02668 Warszawa, Poland; laszcz@ite.waw.pl (A.Ł); aczerwin@ite.waw.pl (A.C.)
6 Chemical Engineering, University of Iceland, IS-107 Reykjavik, Iceland; cpr@hi.is
* Correspondence: mirfray@zut.edu.pl (M.E.F.); roman.sobolewski@rochester.edu (R.S.); Tel.: +48-91-449-4828 (M.E.F.); +1-585-275-1551 (R.S.)
† Current address: Center for Physical Sciences and Technology, LT-10257 Vilnius, Lithuania.

Received: 29 November 2018; Accepted: 14 January 2019; Published: 23 January 2019

Featured Application: We describe the use of terahertz (THz) time-domain spectroscopy to characterize the dispersion of graphene nanoflakes, within a multiblock copolyester matrix. This method probes the dielectric properties of the sample in an almost cm2 cross-section beam path, thereby providing "global" information regarding the dispersion of graphene and its in-situ electronic quality. Because it is a non-destructive testing method, THz time-domain spectroscopy holds great potential for monitoring any nanofiller dispersion in a polymer matrix throughout the product development chain: After polymer nanocomposite synthesis, following processing into a given prototype, and even after product testing.

Abstract: The terahertz time-domain spectroscopy (THz-TDS) technique has been used to obtain transmission THz-radiation spectra of polymer nanocomposites containing a controlled amount of exfoliated graphene. Graphene nanocomposites (1 wt%) that were used in this work were based on poly(ethylene terephthalate-ethylene dilinoleate) (PET-DLA) matrix and were prepared via a kilo-scale (suitable for research and development, and prototyping) in-situ polymerization. This was followed by compression molding into 0.3-mm-thick and 0.9-mm-thick foils. Transmission electron microscopy (TEM) and Raman studies were used to confirm that the graphene nanoflakes dispersed in a polymer matrix consisted of a few-layer graphene. The THz-radiation transients were generated and detected using a low-temperature–grown GaAs photoconductive emitter and detector, both excited by 100-fs-wide, 800-nm-wavelength optical pulses, generated at a 76-MHz repetition rate by a Ti:Sapphire laser. Time-domain signals transmitted through the nitrogen, neat polymer reference, and 1-wt% graphene-polymer nanocomposite samples were recorded and subsequently converted into the spectral domain by means of a fast Fourier transformation. The spectral range of our spectrometer was up to 4 THz, and measurements were taken at room temperature in a dry nitrogen environment. We collected a family of spectra and, based on Fresnel equations, performed a numerical analysis, that allowed us to extract the THz-frequency-range refractive index and absorption coefficient and their dependences on the sample composition and graphene content. Using

the Clausius-Mossotti relation, we also managed to estimate the graphene effective dielectric constant to be equal to ~7 ± 2. Finally, we extracted from our experimental data complex conductivity spectra of graphene nanocomposites and successfully fitted them to the Drude-Smith model, demonstrating that our graphene nanoflakes were isolated in their polymer matrix and exhibited highly localized electron backscattering with a femtosecond relaxation time. Our results shed new light on how the incorporation of exfoliated graphene nanoflakes modifies polymer electrical properties in the THz-frequency range. Importantly, they demonstrate that the complex conductivity analysis is a very efficient, macroscopic and non-destructive (contrary to TEM) tool for the characterization of the dispersion of a graphene nanofiller within a copolyester matrix.

Keywords: graphene; graphene nanoflakes; graphene-polymer nanocomposites; multiblock copolyesters; terahertz time-domain spectroscopy; Drude–Smith model for complex conductivity

1. Introduction

Polymer nanocomposites are prepared by including a nanofiller (carbon, ceramic, metal/metal oxide, and/or others) in a polymer matrix in order to alter (or improve) its properties, such as mechanical, electrical, and optical properties, barrier properties, flame resistance, etc. [1]. Recently, a great deal of interest has been focused on carbon nanofillers and, in particular, graphene. Graphene is a two-dimensional (2-D) nanomaterial consisting of sheets of carbon atoms bonded by sp^2 bonds in a hexagonal configuration: Its unique mechanical, electrical, thermal, and optical properties have been extensively studied [2]. These properties have been leveraged in the development of a wide range of different graphene-polymer nanocomposites [3] using a variety of fabrication methods and polymer types for numerous structural and functional applications [4], including, e.g., biomedical devices [5], biosensing [6], and gas barrier membranes [7].

The key distinguishing feature of nano-fillers, as compared with microscale or conventional fillers, is the very high surface-to-volume ratio inherent in their nanoscale size. Therefore, nano-fillers can have an increased interfacial interaction with the polymer matrix, despite being present at very low concentrations (<5 wt%). In this context, along with the size, the dispersion of the nanofiller in the matrix plays a central role in governing the resulting nanocomposite properties [8]. Generally, it is advantageous for a nanofiller to be well dispersed within the polymer matrix; however, in the case of carbon nanofillers, graphene, and graphite nanoplatelets in particular, obtaining high-quality dispersions without aggregation is a major challenge and limitation [4]. Further, control over the dispersion—to obtain ordered or hierarchical organization of the nanofiller within the polymer matrix—holds breakthrough potential [8].

At present, electron microscopy—transmission electron microscopy (TEM) in particular—remains the gold standard for assessing the dispersion of a nanofiller, because it gives a direct nanofiller image of the dispersion and morphology and can offer density quantification [9]. This approach is limited, however, by the fact that it presents only very local information from select fields of view that are always 2-D. As a result, other methods are being investigated, such as x-ray diffraction and small-angle scattering [10], modulated temperature differential scanning calorimetry [11], ultrasonic dynamic mechanical analysis [12], or dynamic rheological analysis [13]. While each of these methods has distinct advantages, none of them can be used on an object or component of a device because they all require dedicated sample preparation and are often destructive. As a result, these methods cannot be used to assess a nanocomposite after it has been processed into its application state without alteration. However, polymer processing methods—and especially industrially and economically viable methods, such as injection or compression molding—have a definite impact on the properties of a given nanocomposite [14], including the dispersion of a nanofiller.

Terahertz time-domain spectroscopy (THz-TDS) offers an alternative as a non-destructive method suitable for testing even relatively large specimens. THz-TDS has already demonstrated its potential for materials characterization [15], including non-destructive testing (NDT) of both polymers [16] and other composite materials [17]. For example, it has been used to assess damage or detect defects in aeronautic components [18,19]. Further, several groups have proposed using this approach to analyze carbon nanotube and/or graphene-polymer nanocomposites to assess the level of dispersion of the nanofiller [20–24].

Here, we report the use of a THz-TDS technique to characterize graphene nanofiller dispersion within multi-block copolyester nanocomposite materials. Both the copolymer matrix and the nanocomposites were developed within the scope of the ElastoKard project in partnership with the Professor Zbigniew Religa Foundation of Cardiac Surgery Development (FRK) to serve as construction materials for extracorporeal heart assist devices in the context of the Polish Artificial Heart Program [25]. We have recently reported the kiloscale (suitable for Research and Development and prototyping) in-situ polymerization synthesis of these materials and their full physicochemical, thermal, and mechanical characterization [26,27]. These co-polymers and nanocomposites have been successfully used to produce prototype extracorporeal heart assist devices (Figure 1a), including the important hemispherical pneumatic membrane composed of the graphene nanocomposite (Figure 1b). Here, the test samples used were processed using the same compression molding process as the prototype pneumatic membrane. To our knowledge, this is the first time that the dispersion of graphene nanoplatelets within a nanocomposite—prepared at an industrially relevant scale and using an economically viable process—has been studied by the THz-TDS method. Consequently, this work serves as important proof of the concept of THz-TDS of nanocomposites within the product development chain. The level of dispersion of graphene nanoflakes within our nanocomposites was assessed based on the THz-range complex conductivity data, fitted using the Drude–Smith model. This THz characterization approach measures and utilizes both the real and the imaginary parts of the dielectric function (or, equivalently, the index of refraction) for both the neat copolymers and graphene nanocomposites, as well as the amount of THz radiation absorbed as the THz probe beam propagates through the sample.

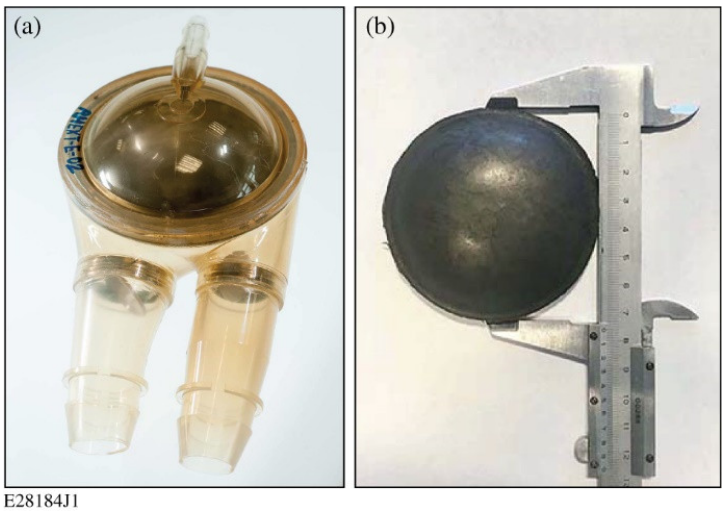

Figure 1. (**a**) Prototype of extracorporeal heart assist device (reprinted with permission [27], copyright 2018, Elsevier); (**b**) graphene nanocomposite pneumatic membrane (calipers provided for scale).

2. Materials and Methods

2.1. Graphene Nanocomposite Preparation and Characterization

The polymer matrix of the studied nanocomposites consisted of multi-block thermoplastic elastomer consisting of hard segments of poly(ethylene terephthalate) (PET) and soft segments of amorphous fatty acid ester sequences based on di-linoleic acid (DLA). The synthesis of both neat copolymers and nanocomposites was carried out in two stages, based on our previous work [26–28], in a kilo-scale (3.5-dm^3) Fourné Maschinenbau polycondensation reactor. Briefly, the first stage consisted of transesterification of dimethyl terephthalate (DMT) and ethylene glycol (EG), followed by esterification with DLA, and, finally, polycondensation. After the completion of the reaction, the polymer was discharged from the reactor in the form of an extruded filament, cooled with water, and cut into granules suitable for further processing, such as injection or compression molding.

Two different neat co-polymers were prepared with different hard to soft segment ratios, resulting in a more elastic material with 40 wt% of hard segments (PET-DLA 4060) and a stiffer co-polyester with 60 wt% of hard segments (PET-DLA 6040). Additionally, nanocomposites with the same hard to soft segment ratios but with 1 wt% of a commercial graphite nanoplatelet nanofiller Grade-A0-3 by the Graphene Supermarket were prepared via in-situ polymerization. (The producer indicates that the Grade-A0-3 graphene has an average thickness of ~12 nm, representing >30 monolayers; therefore, according to the latest classification [29], the Grade-A0-3 material should be termed as a "graphite nanoplatelet"). The synthesis was carried out in stages, in the same fashion as that of the neat polymer, but the nanofiller was first dispersed in the liquid EG and DLA monomers by a combination of bath and probe sonication and high-speed mixing.

We have already published detailed analyses of these materials [26,27], including Fourier transform infrared spectroscopy (FTIR), proton nuclear magnetic resonance (^{1}H NMR), differential scanning calorimetry (DSC), water contact angle measurement, tensile testing, moisture vapor transmission tests, bacterial adhesion testing, and a cytocompatibility assessment.

For THz-TDS measurements, test samples were prepared using compression molding (Remi-Plast PH10T hot press). For the more elastic PET-DLA 4060 copolymer and nanocomposite specimen, nominally 0.3-mm-thick samples were prepared in the same fashion as the membranes for the prototype heart assist device (Figure 1b): The temperature was 175 °C and the pressure was 6 bar. For the stiffer PET-DLA 6040 copolymer and nanocomposites, the temperature was increased to 230 °C, while pressure remained unchanged, and thicker samples (nominally 0.9 mm thick) were prepared.

After fabrication, our nanocomposite samples were characterized using both a high-resolution TEM (HRTEM) and Raman methods in order to image graphene nanoflakes and estimate their size, dispersion, and a number of graphene layers in a flake. Figure 2 presents representative TEM images obtained using a JEM-2100 JEOL microscope at different magnification levels of the thin, 1-wt% graphene-PET-DLA 4060 nanocomposite sample. Figure 2a is a low-magnification image covering a 10 × 10-μm^2 area showing the density and dispersion of the flakes. In this randomly selected image we can identify 12 nanofiller flakes that are well separated from each other. Besides the one "giant" flake (#1), the other flakes have sizes below 1 μm, so, in rough approximation, they can be treated as independent and non-interacting particles dispersed in a host copolymer matrix. Figure 2b shows a HRTEM image of one of the smallest (7-nm × 130-nm) nanoflakes observed and atomic-scale measurements of interplane distances from two areas that could be well oriented for TEM studies. We can clearly image graphene planes and, in this case, see approximately ten layers. Since the starting nanofiller from Graphene Supermarket consisted of graphite nanoplatelets, HRTEM imaging confirmed that the subsequent process of dispersing this nanofiller in the monomers, followed by in-situ polymerization, had exfoliated the nanoplatelets as expected. The insets showed the individual layers with interlayer distances (calculated based on ten layers) equal to 0.355 nm and 0.362 nm for the top and bottom panels, respectively. In both cases, these values are close to the thickness of a single graphene sheet. We must stress, however, that it is difficult to precisely measure the thickness

of the graphene layers in our nanocomposite samples because flakes embedded within the polymer matrix are randomly oriented and their edges are often folded, making proper orientation of the sample during the TEM study difficult. Therefore, although our TEM images and measurements of the thickness of carbon planes in our nanoflakes are consistent with those of graphene monolayers, we cannot completely exclude the probability of having graphite nanoplatelets in our samples.

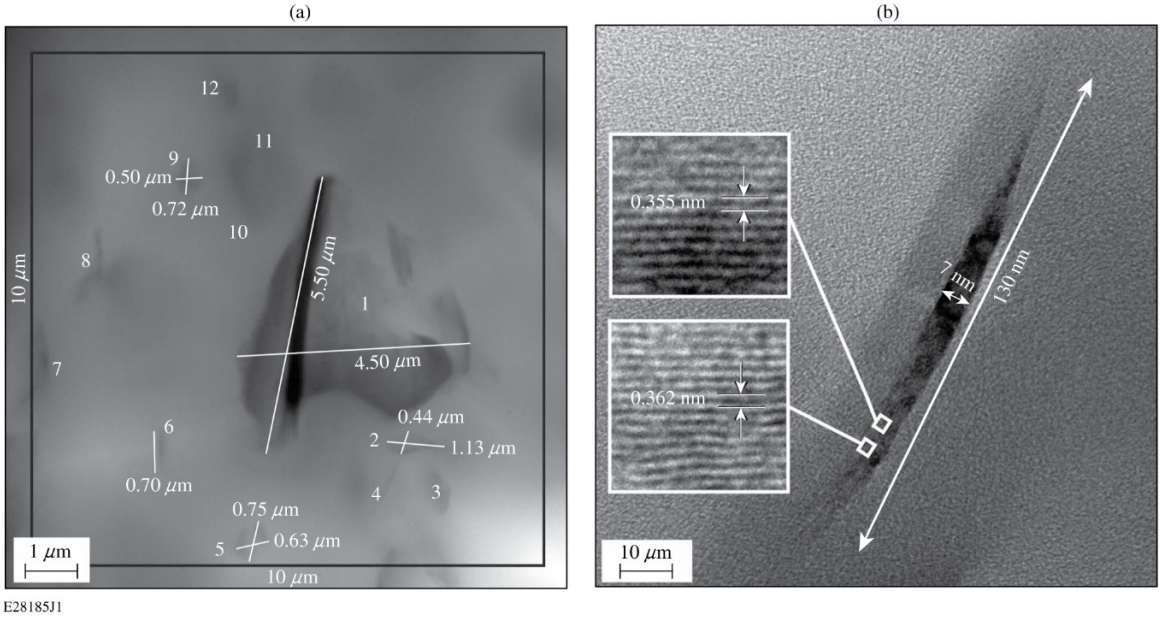

Figure 2. (**a**) Low-resolution (10 × 10-μm^2 area), representative TEM image of 1-wt% graphene PET-DLA 4060 nanocomposite. Twelve (most visible in the view) flakes are identified and the sizes of several flakes are listed. (**b**) HRTEM of the 7-nm × 130-nm nanoflake. Insets show images of graphene planes and interplanar distances from two different sections of the nanoflake (marked as squares).

The above-mentioned ambiguity was resolved by performing scanning fluorescence measurements and Raman spectroscopy. A beam from a helium–neon laser (632.8-nm wavelength) was focused on the sample, and the fluorescence was sent through a 635-nm pass filter (to block the laser line) and was collected by an avalanche photodiode. By scanning the sample using a movable nano-positioning stage, a spatial fluorescence image was created (see inset in Figure 3a). After the scan, the emission was redirected to a spectrometer equipped with a charge-coupled–device (CCD) camera to obtain the Raman spectrum (Figure 3a, main panel). A grating with 600 lines/mm was used to disperse the signal onto the CCD array. The nanoflake under investigation, from which the spectrum was taken, is circled in the inset. The three prominent features visible in the nano-Raman spectrum are the D peak at ~1340 cm^{-1}, the G peak at ~1580 cm^{-1}, and the 2D peak at 2680 cm^{-1}. These features correspond to a few-layer graphene (FLG) sample [29].

We have also performed Raman measurements of an entire 1-wt% graphene-polymer nanocomposite sample, as well as the reference neat PET-DLA 4060 copolymer specimen. Figure 3b shows a spectrum that our graphene nanofiller obtained by numerical subtraction of the neat polymer spectrum from that of the nanocomposite (both shown in the inset in Figure 3b). We note that the positions of the D, G, and 2D peaks very close to that of the nano-Raman study of a single flake. The only difference is the height of the D peak in Figure 3b, which is a defect peak. The discrepancy can be attributed to spectra being collected simultaneously from nanofiller flake edges as well as from within the flake. The edges will increase the observed D band in our spectra. Overall the observed Raman spectra corroborated the fact that, indeed, our nanofiller consisted predominantly of FLG nanoflakes.

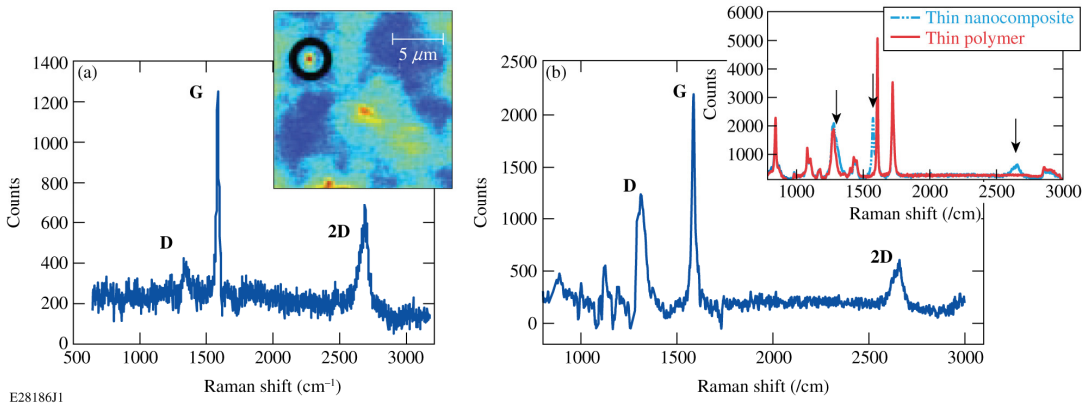

Figure 3. (**a**) Background-subtracted Raman spectrum from a FGL nanoflake embedded in PET-DLA 4060 copolymer matrix. The three prominent features are the D peak at ~1340 cm^{-1}, the G peak at ~1580 cm^{-1}, and the 2D peak at 2680 cm^{-1}. The inset presents a scanning fluorescence image of the region from which the spectrum was taken, with the studied nanoflake circled. For the images, the excitation wavelength was 632.8 nm and the laser power was 600 μW. (**b**) Background-subtracted Raman spectrum of graphene nanoflakes obtained by subtraction of the spectrum of neat PET-DLA 4060 copolymer, used as the graphene nanocomposite matrix. The latter two spectra are both shown in the inset in (**b**), with arrows pointing to the characteristic features of the nanocomposite. The positions of the main peaks in the main panel are the D peak at ~1311 cm^{-1}, the G peak at ~1586 cm^{-1}, and the 2D peak at 2661 cm^{-1}.

2.2. THz Time-Domain Spectroscopy Technique

The THz-TDS system, which is used to measure the THz-range transmission spectra of both the neat copolymers and graphene nanocomposite samples, is schematically presented in Figure 4. THz radiation was generated and detected using a commercial, low-temperature–grown GaAs (LT-GaAs) photo-conductive antenna emitter and detector from TeraVil Ltd., Vilnius, Lithuania [30]. The emitter and detector were excited and probed, respectively, by 100-fs-wide pulses, with 800-nm wavelength and 76-MHz repetition rate, generated by a femtosecond Ti:Sapphire laser. The spectral range of the spectrometer was ~4 THz, with a maximum amplitude of ~0.5 THz. The sample was placed directly between the emitter and detector, as shown in Figure 4, and measurements were taken at room temperature. To reduce the influence of water absorption, the THz emitter, detector, and sample holder were placed inside a Plexiglas® box that was purged with dry nitrogen, ensuring that the humidity during the measurement was below 5%.

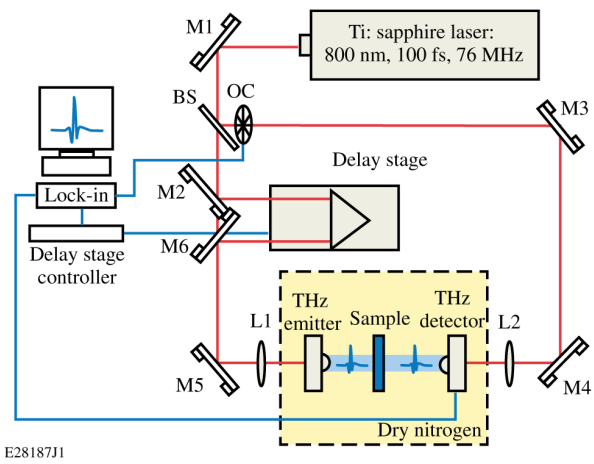

Figure 4. Schematic diagram of a THz-TDS setup. L1, L2: optical lenses; M1–M6: dielectric mirrors; BS: beam splitter, and OC: optical chopper.

For each sample, we first performed a reference run with no sample inside the spectrometer to confirm the performance of the system. Next, we took two measurements; one of a graphene nanocomposite and the other of a corresponding neat co-polymer specimen. To get better results and reduce noise, each set of measurements consisted of at least ten averages. Our measurements were focused on two different sample types: A nominal 0.3-mm-thick, elastic PET-DLA 4060 copolymer and a nominal 0.9-mm-thick, stiff PET-DLA 6040 copolymer. For both sample types, the nanofiller content was the same, i.e., 1 wt%. Since our further analysis crucially depends on the sample thickness, all measurements were repeated several times. At different spots of the test sample, the corresponding local thicknesses were measured, and, subsequently, the results were averaged. Therefore, from now on, we will refer to a nominal 0.3-mm PET-DLA 4060 soft copolymer sample as a "thin sample," and a nominal 0.9-mm PET-DLA 6040 stiff copolymer sample as a "thick sample."

Figure 5a presents the time-domain signals transmitted through dry nitrogen (the reference measurement), the thin and thick neat copolymers, and the corresponding thin and thick, 1-wt% graphene-polymer nanocomposite samples, respectively (see the legend for detailed color/line coding). As expected, the transient corresponding to the thick sample with graphene exhibits the smallest amplitude and the longest arrival time to the detector. The differences in time delays, with respect to the nitrogen signal observed in the signals corresponding to different samples, are caused by their different indexes of refraction, as will be discussed later in connection with Figure 6a. In Figure 5b, we present the corresponding (see the legend) power spectra of our time-domain signals obtained by means of fast Fourier transformation (FFT). We note that, while both copolymers absorb THz radiation, as compared to the dry-nitrogen reference signal, adding graphene flakes to the polymer matrix substantially reduces the bandwidth of the power spectrum (Figure 5b), obviously because of the extra absorption of THz radiation by nanoflakes. The cut-off frequencies for the thin copolymer sample and the corresponding 1-wt% graphene-polymer nanocomposite are ~3.1 THz and 2.9 THz, respectively, while for the thick copolymer and the 1-wt% graphene-polymer nanocomposite they are 2.25 THz, and 1.75 THz, respectively. We observe no resonant absorption features, but rather a broadband THz attenuation.

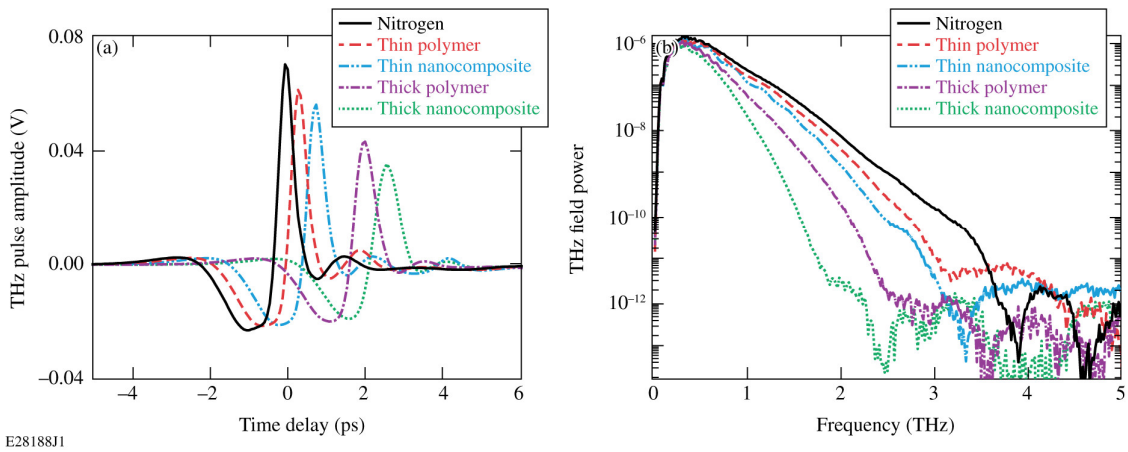

Figure 5. (**a**) Time-resolved transient signals for the tested thin and thick polymers and 1-wt% graphene nanocomposite samples and the empty spectrometer (nitrogen). (**b**) The corresponding power spectra showing absorption of the samples. Note: The thin samples consist of the PET-DLA 4060 copolymer, while the thick ones consist of PET-DLA 6040.

3. Results and Discussion

3.1. Data Analysis

Using Fresnel equations, the THz-TDS approach allows us to find the complex index of refraction $\hat{n}(\omega) = n(\omega) + i\kappa(\omega)$, or the dielectric function $\hat{\varepsilon}(\omega) = \varepsilon_1(\omega) + i\varepsilon_2(\omega)$, of a tested material. The $\hat{\varepsilon}(\omega)$

can be represented as the square of $\hat{n}(\omega)$, i.e., $\hat{\varepsilon}(\omega) = [\hat{n}(\omega)]^2$. When the sample is placed between the THz emitter and detector, the recorded electric field signal $E_{\text{sam}}(t)$ is the THz transient that is transmitted through sample. The reference signal, $E_{\text{ref}}(t)$, is registered when the same measurement is taken, but without the sample. By taking FFT of time-domain transients, we can obtain the frequency-domain spectra of both the sample and reference. When these two spectra are compared, the $\hat{\varepsilon}(\omega)$ and $\hat{n}(\omega)$ dependencies, as well as the absorption coefficient $\alpha(\omega)$, can be calculated.

In agreement with our measurements, we can treat our samples as optically thick materials. In this case, internal reflections do not overlap with the main THz pulse, so, for the sake of simplicity, the data before and after the main pulse can be truncated and only the main THz pulse, analyzed [31]. Consequently, the transmission amplitude ratio $A(\omega)$ and phase difference $\varphi(\omega)$ of sample and reference fields can be calculated as [32],

$$\frac{E_{\text{sam}}(\omega)}{E_{\text{ref}}(\omega)} = \frac{4n(\omega)}{[n(\omega)+1]^2} e^{-\frac{\alpha d}{2} + i\omega \frac{[n(\omega)-1]d}{c}} = A(\omega)e^{i\varphi(\omega)}, \tag{1}$$

where c is the speed of light, d represents the sample thickness, and ω is the angular frequency. From Equation (1) we can derive the absorption coefficient $\alpha(\omega)$ and the real component $n(\omega)$ of $\hat{n}(\omega)$:

$$\alpha(\omega) = -\frac{2}{d} ln\left\{ A(\omega)\frac{[n(\omega)+1]^2}{4n(\omega)} \right\}, \tag{2}$$

$$n(\omega) = 1 + \frac{c}{\omega d}\varphi(\omega). \tag{3}$$

In addition, the extinction coefficient $\kappa(\xi)$ is related to the absorption coefficient as,

$$\kappa(\omega) = \frac{c\alpha(\omega)}{2\omega}. \tag{4}$$

After finding the components of $\hat{n}(\omega)$ and $\hat{\varepsilon}(\omega)$, the complex conductivity $\hat{\sigma}(\omega) = \sigma_1(\omega) + i\sigma_2(\omega)$ of the sample can be subsequently calculated using Equations (5)–(8) [33]:

$$\varepsilon_1(\omega) = n(\omega)^2 - \kappa(\omega)^2, \tag{5}$$

$$\varepsilon_2(\omega) = 2n(\omega)\kappa(\omega), \tag{6}$$

$$\sigma_1(\omega) = 2\varepsilon_0\omega n(\omega)\kappa(\omega), \tag{7}$$

$$\sigma_2(\omega) = \left[\varepsilon_{\text{pl}}(\omega) - n(\omega)^2 + \kappa(\omega)^2\right]\varepsilon_0\omega, \tag{8}$$

where ε_0 is the permittivity of the free space, and $\varepsilon_{\text{pl}}(\omega)$ is the dielectric constant of a neat polymer matrix. We assume that imaginary part ε_{p2} is negligibly small since the neat polymer is an insulating material. $\varepsilon_{\text{pl}}(\omega)$ can be extracted from THz-TDS measurements of a neat polymer in dry nitrogen using the same routine as presented above for the graphene-polymer nanocomposite (using Equations (1)–(5)).

3.2. Index of Refraction and Absorption Coefficient

As mentioned before, we studied two sets of samples: Thin (nominal 0.3 mm) and thick (nominal 0.9 mm); each set contained a different co-polymer as reference and 1-wt% graphene nanocomposite. Since the sample thickness is a very important parameter for calculating $\hat{n}(\omega)$ and $\varepsilon(\omega)$, we repeated our measurements several times at different spots on a given sample and used the averaged value for the sample parameter calculation. Spectral dependencies of $n(\omega)$ and $\alpha(\omega)$ obtained from the THz-TDS data, using Equations (2) and (3), are presented in Figure 6a,b, respectively.

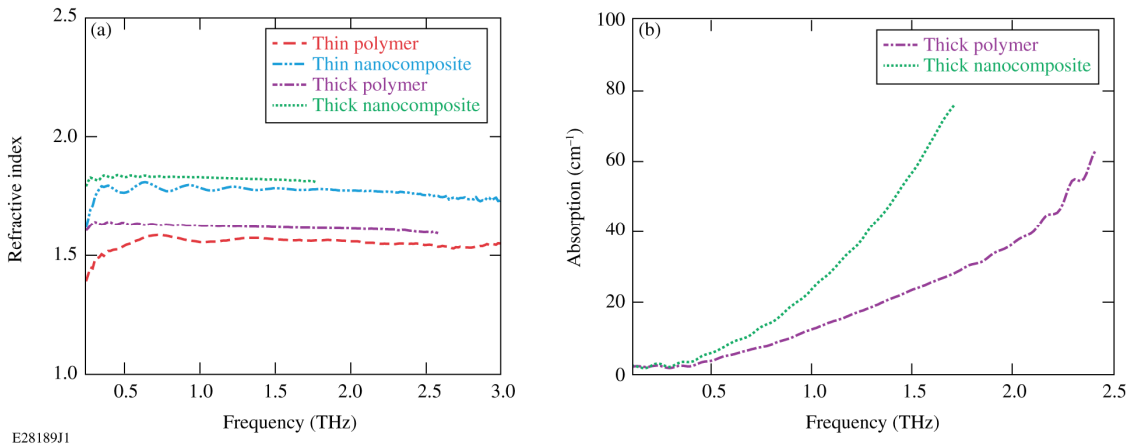

Figure 6. (**a**) Index of refraction and (**b**) absorption spectra for the tested neat copolymer and 1-wt% graphene nanocomposite samples. Note: The thin sample consisted of PET-DLA 4060 copolymer, while the thick one consisted of PET-DLA 6040. The data points were trimmed according to sample bandwidth (see Figure 5b).

One should ignore the low-frequency oscillations in the extracted $n(\omega)$ and $\alpha(\omega)$ spectra (Figure 6), that are the most pronounced for the thin samples because these oscillations can be attributed to the approximation error of our simplified model. The methodology behind Equation (1) requires that the time-domain signal be truncated before any secondary peaks (because of internal reflections). This truncation, as well as minor deviation or inaccuracy in the sample thickness determination, introduces an incomplete removal of the Fabry–Pérot reflections of the THz signal, resulting in observed oscillations. Note that the oscillations for the thick samples are much smaller and have a smaller period, which is consistent with this approximation error. These errors, while relatively small in the $n(\omega)$ spectra, were very substantial in the calculated $\alpha(\omega)$ spectrum for the thin samples and, eventually, prevented us from obtaining a consistent plot in the latter case.

The $n(\omega)$ spectra of both neat copolymers, as seen in Figure 6a, are almost flat across the entire measured range, and the values at 1 THz for a thin and a thick polymer are ~1.57 and ~1.62, respectively, which are close to the values observed earlier for PET polymer [34,35]. The different $n(\omega)$ values for the thin and thick samples are caused by the different ratio between the hard and soft segments in the PET-DLA 4060 and PET-DLA 6040 copolymers. The PET-DLA 6040 co-polymer has a higher percentage of PET hard segments and therefore a higher crystallinity, resulting in the increased n value. When 1 wt% of graphene nanofiller was added into each copolymer, the $n(\omega)$ dependences of the resultant nanocomposites remained flat in the measurement range, but the values, again evaluated at 1 THz, increased to ~1.78 and ~1.83 for the thin and thick samples, respectively. Clearly, adding 1 wt% of graphene flakes to a copolymer matrix measurably increased (~10%) the n of the resultant nanocomposite. Similar results were obtained by other groups [21,22].

As explained above, Figure 6b shows $\alpha(\omega)$ spectra for only the thick samples, i.e., the neat PET-DLA 6040 co-polymer and the corresponding graphene nanocomposite. The addition of 1-wt% graphene into the copolymer matrix increases the $\alpha(\omega)$, especially at the high-frequency end of the spectrum. The latter result is in good agreement with previously published data [22].

3.3. Dielectric Constant

Knowing the $n(\omega)$ dependence, it is easy to calculate the spectra for the relative dielectric constant $\varepsilon_1(\omega)$ for both the neat co-polymer and the graphene nanocomposite, for both the thin and thick samples, as shown in Figure 7a,b, respectively. The resulting $\varepsilon_1(\omega)$ spectra are flat, as we observed earlier for the $n(\omega)$ dependences presented in Figure 6a. The insertion of graphene nanoflakes increases the dielectric constant of the corresponding nanocomposite sample. Despite a very large frequency

difference, our numerical values of $\varepsilon_1(\omega)$ are close to those reported by Marra et al. [21], measured at radio frequencies from 8 to 12 GHz.

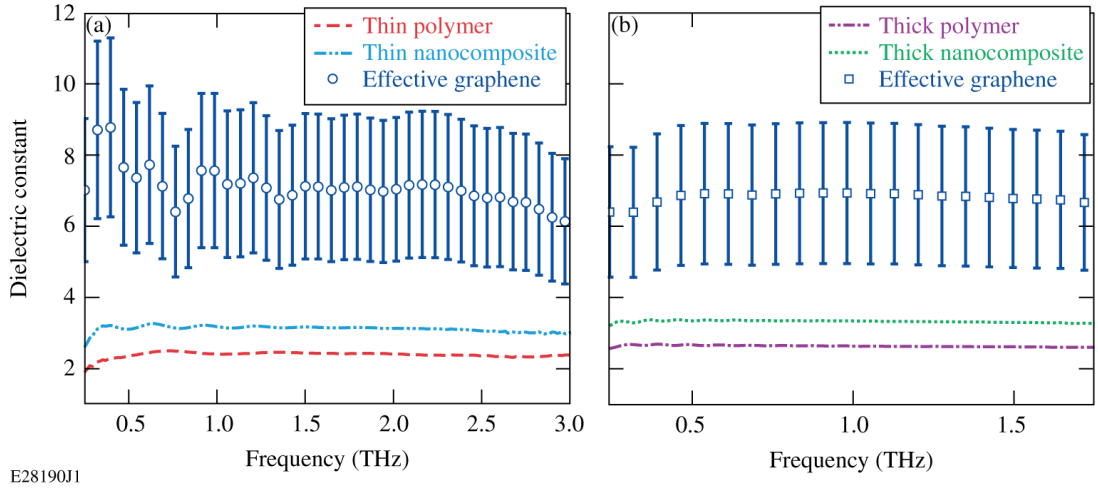

Figure 7. Real part of the complex dielectric function spectra (solid lines) for (**a**) thin and (**b**) thick polymer and 1-wt% graphene nanocomposite samples. Note: The thin samples consist of PET-DLA 4060 copolymer, while the thick one was PET-DLA 6040. The open circle and open square symbols present the effective graphene flake dielectric function based on the Clausius–Mossotti relation. The error bars are ~30%.

The $\varepsilon_1(\omega)$ spectra presented in Figure 7 were subsequently used to estimate the dielectric constant of only graphene flakes embedded in the polymer. Our approach is based on the classical Clausius–Mossotti relation that describes the dielectric constant of a composite sample ε_c [36] as

$$\varepsilon_c(\omega) = \frac{3\varepsilon_{\mathrm{pl}}(\omega) + 2N\alpha}{3\varepsilon_{\mathrm{pl}}(\omega) - N\alpha}\varepsilon_{\mathrm{pl}}(\omega), \tag{9}$$

where N represents the density of the graphene nanoflakes and α in this case, is a so-called "atomic polarizability". We note here that the effective-medium theory of Bruggeman, most commonly used for the composite material analysis, are not applicable here since it requires that volume fraction of a filler material be at least 10% [37]. This condition is, obviously, not fulfilled in our case because we have only 1 wt% of graphene nanoflakes in the copolymer matrix. On the other hand, based on the TEM images (see Figure 2a), the graphene nanoflakes in our samples are well separated from each other. Consequently, we can assume that they act as independent and noninteracting particles in a host material and use the Clausius–Mossotti relation that is the exact solution of a dielectric constant of a medium having classically interacting dipoles embedded in an insulating matrix. Therefore, we simply treat each flake as a dipole and the dielectric constant of graphene nanoflakes $\varepsilon_{gr}(\omega)$ should be proportional to $N\alpha$ and given as

$$\varepsilon_{\mathrm{gr}}(\omega) = N\alpha * \frac{1}{\delta}, \tag{10}$$

where δ is the volume ratio of graphene nanoflakes to the entire sample volume. Of course, the 1-wt% ratio does not reflect the volume ratio, so we used the TEM images of our samples (see Figure 2a) to estimate the volume percentage of the randomly distributed and orientated graphene nanoflakes inside our nanocomposite. The calculation results of $\varepsilon_{gr}(\omega)$ are shown in Figure 7 as symbols. The error bars represent an uncertainty of ~30% in our evaluation of δ. Comparing the results presented in Figure 7a,b, we see that ignoring the low-frequency section of $\varepsilon_{gr}(\omega)$ for the thin sample (mentioned in earlier Fabry–Pérot reflections), the $\varepsilon_{gr}(\omega)$ values for both graphene nanocomposite samples are very close to each other and are ~7 ± 2.

3.4. Complex Conductivity

The complex conductivity calculations are based on Equations (7) and (8). In order to calculate the complex $\hat{\sigma}(\omega)$ of our graphene nanocomposite samples, we need to know the complex dependences of $\hat{\varepsilon}(\omega)$ for not only the nanocomposite, but also for the neat polymer matrix. Therefore, we additionally calculated the $\hat{\varepsilon}(\omega)$ spectrum for each neat copolymer sample, using Equations (1)–(6), with the reference corresponding to the THz transient spectrum measured in dry nitrogen. The resulting real and imaginary parts of the graphene nanocomposite complex conductivity are plotted as symbols for both the thin (open circles) and thick (open triangles) in Figure 8. To calculate error bars, we analyzed the data collected in different sets of measurements performed at different spots on our samples.

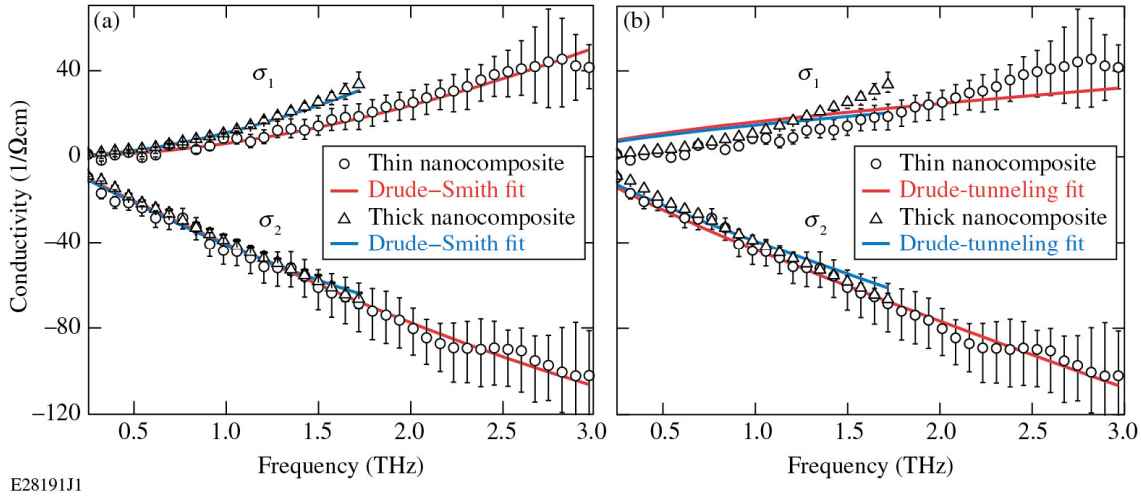

Figure 8. Experimental complex conductivity (σ_1 and σ_2) spectra for both thin (open circles) and thick (open triangles), 1-wt% graphene nanocomposite samples. Solid lines correspond to the fits based (**a**) the Drude–Smith and (**b**) Drude-tunneling models. Experimental data points for the thick sample were trimmed according to sample bandwidth (see Figure 5b).

Next, our $\hat{\sigma}(\omega)$ spectra were fitted using the Drude–Smith model [38] (solid lines in Figure 8a), and what we call the Drude-tunneling model presented in [39] (solid lines in Figure 8b). The Drude–Smith model is given by

$$\sigma(\omega) = \frac{\varepsilon_0 \omega_p^2 \tau}{(1 - i\omega\tau)} \left[1 + \sum_{m=1}^{\infty} \frac{c_m}{(1 - i\omega\tau)} \right], \tag{11}$$

where ω_p is the plasma frequency, τ represents the carrier collision time, and the c_m coefficient is the so-called scattering parameter. A first-order approximation is conventionally used, i.e., the terms $m > 1$ are truncated. When $c_m = 0$, Equation (11) simplifies to the classical Drude model (the term in front of the square bracket), while $c_1 = -1$ means that carriers are completely backscattered. This extension of the classic Drude model was introduced by Smith [38] and is usually used to describe complex conductivity spectra in the THz range of materials with nanofillers [40], such as nanoparticles [41,42], carbon nanotubes [43], and even monolayer graphene [43], when it is difficult to explain results using the simple, homogeneous-medium Drude model.

The model presented in [39] is based on a concept that in non-homogeneous, granular materials carrier transport consists of both, intragrain scattering and intergrain tunneling, and the corresponding $\sigma_{eff}(\omega)$ should be described, in general, as a superposition of both processes and given by as

$$\frac{1}{\sigma_{eff}(\omega)} = \frac{f}{\sigma_f(\omega)} + \frac{1 - f}{\sigma_t(\omega)}, \tag{12}$$

where $\sigma_f(\omega)$ is the free carrier conductivity given by the Drude law (m = 0 in Equation (11)), $\sigma_t(\omega)$ is the tunneling conductivity given in [39], and f is the spectral weight of intragrain transport. The latter explains why the authors in [39] call this approach the free (intra-grain) and tunneling (inter-grain; grain boundary) carrier transport model.

Analyzing Figure 8a, we observe that we obtained an excellent fit using, as it is a standard procedure, only the first term (m = 1) in the Smith expansion (Equation (11)) and the fitting parameters were $c_1 = -0.997$, $\omega_p = 72.4 \times 10^{12}$ 1/s, and τ = 12 fs for the thin nanocomposite sample, and $c_1 = -0.998$, $\omega_p = 41.9 \times 10^{12}$ 1/s, and τ = 21 fs for the thick one (in both cases, the $\omega_p\tau$ product is approximately the same and equal to 0.87). We observe that in both cases, the c_1 values are very close to -1, indicating a nearly complete backscattering mechanism of carriers inside our graphene-polymer samples.

In the case of Figure 8b, the fit based on the Drude-tunneling model (Equation (12)) is not as good, especially in the case of σ_1, and we need to stress that it was obtained for f = 0.98, i.e., the tunneling process is almost negligible in our case. The latter, combined with the fact that for both the thin and thick nanocomposite samples, σ_2 is negative in the entire frequency range, points to that in our nanocomposites (based on either PET-DLA 4060 or PET-DLA 6040 copolymers) the graphene nanofiller is well-distributed, and consists of individual conducting nanoflakes that are well isolated from each other inside a polymer matrix.

Using the Drude–Smith best-fit ω_p parameters, and by experimentally-determining the graphene layer-to-layer separation distance (see Figure 2b), we estimated the free-carrier concentration in our nanoflakes to be equal to ~1.1×10^9 cm^{-2} and ~3.2×10^9 cm^{-2} for the thick, and thin sample, respectively. The ultrashort carrier collision time τ obtained from the Drude–Smith model indicates, in turn, that our graphene nanoflakes are, on average, much larger than the carrier mean-free path within the flake, estimated to be on the order of 10 nm. The latter confirms the applicability of the Drude-Smith approach to model the carrier transport in our graphene-polymer nanocomposites. Finally, we point to very similar THz conductivity studies, very recently reported by Skalsky et al. [22]. The authors used samples consisting of FLG flakes embedded in polytetrafluoroethylene (PTFE) pellets, and measured them using the THZ-TDS method. They fitted only the σ_1 spectrum, but also obtained c_1 very close to -1 and very similar free-carrier concentration, as well as came to very similar conclusions as ours.

4. Conclusions

We have successfully used THz time-domain spectroscopy to characterize multi-block, co-polyester, graphene nanocomposite materials, synthesized using kilo-scale (suitable for Research and Development, and prototyping) in-situ polymerization and processed using industrially/economically viable compression molding. We present an experimental procedure and step-by-step data workup method used to characterize the FLG nanofiller within an insulating matrix material for the case where the filler is at relatively low density (1 wt%). We have shown that one can extract the refractive index, the dielectric constant, and the complex conductivity of the graphene-polymer nanocomposite material, as well as the effective dielectric constant of graphene nanoflakes within the matrix. In the THz-TDS method, the dielectric properties represent a sample average of all the materials in an almost cm^2 cross-section beam path; consequently, these data contain "global" information regarding the dispersion of the filler (in our case FLG) and its final retained "quality." In our study, the Drude–Smith backscatter parameter, which is close to -1, and the negative imaginary part of the complex conductivity both indicate that our nanofiller flakes are fully isolated in the polymer matrix. The quality of the dispersion is implied by the high value of the conductivity and moderate effective dielectric constant that is retained by the graphene nanoflakes. High THz conductivity typically corresponds to high carrier mobility within individual graphene flakes, which in turn suggests that flakes are structurally intact, without a significant amount of scattering defects introduced. The results of our THz study are consistent with the HRTEM image analysis, and indicate that THz-TDS characterization is uniquely suited to probe the dispersion and in-situ electronic quality of nanofillers such as graphene or, e.g., carbon-nanotubes in various, not only polymer, composite

materials. In the latter context, however, it is important to stress that tested elastic PET-DLA 4060 copolymer nanocomposites are analogous to experimental hemispherical pneumatic membranes of a prototype extra-corporeal heart assist device (Figure 1). Consequently, this work, as well as other similar THz studies, serves as an important proof of concept of THz spectroscopy of nanocomposites in the product development chain. Non-destructive measurements could be carried out at different stages of the process: Aafter polymer nanocomposite synthesis, following processing into a given prototype component, and even after "field" testing (either mechanical or functional).

Author Contributions: Conceptualization, M.E.F. and R.S.; methodology, A.K., Z.S., P.S., and C.P.R.; investigation, A.K., G.C., K.M.G., Z.S., and A.Ł.; formal analysis, A.K., G.C. P.S., and C.P.R.; validation, A.N.V., M.E.F., A.C., and R.S.; visualization, A.K., G.C., K.M.G., and A.Ł.; resources, A.N.V., M.E.F., A.C., and R.S.; writing—original draft preparation, A.K., G.C., P.S., C.P.R., and R.S.; writing—review and editing, A.K., A.N.V., P.S., M.E.F., A.Ł., C.P.R., and R.S.; supervision, R.S.; project administration, A.N.V., M.E.F., A.C., and R.S.; funding acquisition, A.N.V., M.E.F., A.C., and R.S.

Funding: This research was funded in part by the PumpPrimerII Program at the University of Rochester. A.N.V. acknowledges support from the Air Force Office of Scientific Research (FA9550-16-1-0020). M.E.F. acknowledges support from the Polish National Centre for Research and Development (PBS1/A5/2/2012).

Acknowledgments: P. Sobolewski thanks W. Ignaczak from the West Pomeranian University of Technology for their helpful discussions.

Conflicts of Interest: The authors declare no conflict of interest. The funders had no role in the design of the study; in the collection, analyses, or interpretation of data; in the writing of the manuscript, or in the decision to publish the results.

References

1. Paul, D.R.; Robeson, L.M. Polymer nanotechnology: Nanocomposites. *Polymer* **2008**, *49*, 3187–3204. [CrossRef]
2. Zhu, Y.; Murali, S.; Cai, W.; Li, X.; Suk, J.W.; Potts, J.R.; Ruoff, R.S. Graphene and graphene oxide: Synthesis, properties, and applications. *Adv. Mater.* **2010**, *22*, 3906–3924. [CrossRef] [PubMed]
3. Potts, J.R.; Dreyer, D.R.; Bielawski, C.W.; Ruoff, R.S. Graphene-based polymer nanocomposites. *Polymer* **2011**, *52*, 5–25. [CrossRef]
4. Hu, K.; Kulkarni, D.D.; Choi, I.; Tsukruk, V.V. Graphene-polymer nanocomposites for structural and functional applications. *Prog. Polym. Sci.* **2014**, *39*, 1934–1972. [CrossRef]
5. Silva, M.; Alves, N.M.; Paiva, M.C. Graphene-polymer nanocomposites for biomedical applications. *Polym. Adv. Technol.* **2018**, *29*, 687–700. [CrossRef]
6. Sobolewski, P.; Piwowarczyk, M.; Fray, M.E. Polymer-graphene nanocomposite materials for electrochemical biosensing. *Macromol. Biosci.* **2016**, *16*, 944–957. [CrossRef] [PubMed]
7. Cui, Y.; Kundalwal, S.I.; Kumar, S. Gas barrier performance of graphene-polymer nanocomposites. *Carbon* **2016**, *98*, 313–333. [CrossRef]
8. Kumar, S.K.; Benicewicz, B.C.; Vaia, R.A.; Winey, K.I. 50th anniversary perspective: Are polymer nanocomposites practical for applications? *Macromolecules* **2017**, *50*, 714–731. [CrossRef]
9. Khare, H.S.; Burris, D.L. A quantitative method for measuring nanocomposite dispersion. *Polymer* **2010**, *51*, 719–729. [CrossRef]
10. Schaefer, D.W.; Justice, R.S. How nano are nanocomposites? *Macromolecules* **2007**, *40*, 8501–8517. [CrossRef]
11. Miltner, H.E.; Watzeels, N.; Goffin, A.-L.; Duquesne, E.; Benali, S.; Dubois, P.F.; Rahier, H.; Van Mele, B. Quantifying the degree of nanofiller dispersion by advanced thermal analysis: Application to polyester nanocomposites prepared by various elaboration methods. *J. Mater. Chem.* **2010**, *20*, 9531–9542. [CrossRef]
12. Espinoza-González, C.; Ávila-Orta, C.; Martínez-Colunga, G.; Lionetto, F.; Maffezzoli, A. A measure of CNTs dispersion in polymers with branched molecular architectures by UDMA. *IEEE Trans. Nanotechnol.* **2016**, *15*, 731–737. [CrossRef]
13. Zhang, Q.; Fang, F.F.; Zhao, X.P.; Li, Y.; Zhu, M.; Chen, D. Use of dynamic rheological behavior to estimate the dispersion of carbon nanotubes in carbon nanotube/polymer composites. *J. Phys. Chem. B* **2008**, *112*, 12606–12611. [CrossRef] [PubMed]

14. Müller, K.-H.; Bugnicourt, E.; Latorre, M.; Jorda, M.; Echegoyen Sanz, Y.; Lagaron, J.; Miesbauer, O.; Bianchin, A.; Hankin, S.; Bölz, U.; et al. Review on the processing and properties of polymer nanocomposites and nanocoatings and their applications in the packaging, automotive and solar energy fields. *Nanomaterials* **2017**, *7*, 74. [CrossRef] [PubMed]
15. Naftaly, M.; Miles, R.E. Terahertz time-domain spectroscopy for material characterization. *Proc. IEEE* **2007**, *95*, 1658–1665. [CrossRef]
16. Wietzke, S.; Jansen, C.; Reuter, M.; Jung, T.; Kraft, D.; Chatterjee, S.; Fischer, B.M.; Koch, M. Terahertz spectroscopy on polymers: A review of morphological studies. *J. Mol. Struct.* **2011**, *1006*, 41–51. [CrossRef]
17. Amenabar, I.; Lopez, F.; Mendikute, A. In introductory review to THz non-destructive testing of composite mater. *J. Infrared Millim. Terahertz Waves* **2013**, *34*, 152–169. [CrossRef]
18. Stoik, C.; Bohn, M.; Blackshire, J. Nondestructive evaluation of aircraft composites using reflective terahertz time domain spectroscopy. *NDT&E Int.* **2010**, *43*, 106–115.
19. Ospald, F.; Zouaghi, W.; Beigang, R.; Matheis, C.; Jonuscheit, J.; Recur, B.; Guillet, J.-P.; Mounaix, P.; Vleugels, W.; Bosom, P.N.; et al. Aeronautics composite material inspection with a terahertz time-domain spectroscopy system. *Opt. Eng.* **2013**, *53*, 031208. [CrossRef]
20. Casini, R.; Papari, G.; Andreone, A.; Marrazzo, D.; Patti, A.; Russo, P. Dispersion of carbon nanotubes in melt compounded polypropylene based composites investigated by THz spectroscopy. *Opt. Express* **2015**, *23*, 18181–18192. [CrossRef]
21. Marra, F.; D'Aloia, A.; Tamburrano, A.; Ochando, I.; De Bellis, G.; Ellis, G.; Sarto, M. Electromagnetic and dynamic mechanical properties of epoxy and vinylester-based composites filled with graphene nanoplatelets. *Polymers* **2016**, *8*, 272. [CrossRef]
22. Skalsky, S.; Molloy, J.; Naftaly, M.; Sainsbury, T.; Paton, K.R. Terahertz time-domain spectroscopy as a novel metrology tool for liquid-phase exfoliated few-layer graphene. *Nanotechnology* **2018**, *30*, 025709. [CrossRef] [PubMed]
23. Chamorro-Posada, P.; Vázquez-Cabo, J.; Rubiños-López, O.; Martín-Gil, J.; Hernández-Navarro, S.; Martín-Ramos, P.; Sánchez-Arévalo, F.M.; Tamashausky, A.V.; Merino-Sánchez, C.; Dante, R.C. THz TDS study of several sp^2 carbon materials: Graphite, needle coke and graphene oxides. *Carbon* **2018**, *98*, 484–490. [CrossRef]
24. Whelan, P.R.; Huang, D.; Mackenzie, D.; Messina, S.A.; Li, Z.; Li, X.; Li, Y.; Booth, T.J.; Jepsen, P.U.; Shi, H.; et al. Conductivity mapping of graphene on polymeric films by terahertz time-domain spectroscopy. *Opt. Express* **2018**, *26*, 17,748–17,754. [CrossRef] [PubMed]
25. El Fray, M.; Czugala, M. Polish artificial heart program. *WIREs Nanomed. Nanobiotechnol.* **2012**, *4*, 322–328. [CrossRef] [PubMed]
26. Staniszewski, Z.; El Fray, M. Influence of thermally exfoliated graphite on physicochemical, thermal and mechanical properties of copolyester nanocomposites. *Polimery* **2016**, *61*, 482–489. [CrossRef]
27. Staniszewski, Z.; Sobolewski, P.; Piegat, A.; El Fray, M. The effects of nano-sized carbon fillers on the physico-chemical, mechanical, and biological properties of polyester nanocomposites. *Eur. Polym. J.* **2018**, *107*, 189–201. [CrossRef]
28. Piegat, A.; El Fray, M. Polyethylene terephthalate modification with the monomer from renewable resources. *Polimery* **2007**, *52*, 885–888. [CrossRef]
29. Kauling, A.P.; Seefeldt, A.T.; Pisoni, D.P.; Pradeep, R.C.; Bentini, R.; Oliveira, R.V.B.; Novoselov, K.S.; Castro Neto, A.H. The worldwide graphene flake production. *Adv. Mater.* **2018**, *30*, 1803784. [CrossRef]
30. Geižutis, A.; Krotkus, A.; Bertulis, K.; Molis, G.; Adomavičius, R.; Urbanowicz, A.; Balakauskas, S.; Valaika, S. Terahertz radiation emitters and detectors. *Opt. Mater.* **2008**, *30*, 786–788. [CrossRef]
31. Duvillaret, L.; Garet, F.; Coutaz, J.-L. Highly precise determination of optical constants and sample thickness in terahertz time-domain spectroscopy. *Appl. Opt.* **1999**, *38*, 409–415. [CrossRef] [PubMed]
32. Fischer, B.M.; Helm, H.; Jepsen, P.U. Chemical recognition with broadband THz spectroscopy. *Proc. IEEE* **2007**, *95*, 1592–1604. [CrossRef]
33. Zou, X.; Shang, J.; Leaw, J.; Luo, Z.; Luo, L.; La-o-vorakiat, C.; Cheng, L.; Cheong, S.A.; Su, H.; Zhu, J.-X.; et al. Terahertz conductivity of twisted bilayer graphene. *Phys. Rev. Lett.* **2013**, *110*, 067401. [CrossRef] [PubMed]
34. Jin, Y.S.; Kim, G.J.; Jeon, S.G. Terahertz dielectric properties of polymers. *J. Korean Phys. Soc.* **2006**, *49*, 513–517.

35. Fedulova, E.V.; Nazarov, M.M.; Angeluts, A.A.; Kitai, M.S.; Sokolov, V.I.; Shkurinov, A.P. Studying of dielectric properties of polymers in the terahertz frequency range. *Proc. SPIE* **2012**, *8337*, 83370I.
36. Talebian, E.; Talebian, M. A general review on the derivation of Clausius–Mossotti relation. *Optik* **2013**, *124*, 2324–2326. [CrossRef]
37. Scheller, M.; Jansen, C.; Koch, M. Applications of effective medium theories in the terahertz regime. In *Recent Optical and Photonic Technologies*; Kim, K.Y., Ed.; IntechOpen: London, UK, 2010; pp. 231–250.
38. Smith, N.V. Classical generalization of the Drude formula for the optical conductivity. *Phys. Rev. B* **2001**, *64*, 155106. [CrossRef]
39. Shimakawa, K.; Kasap, S. Dynamics of carrier transport in nanoscale materials: Origin of non-Drude behavior in the terahertz frequency range. *Appl. Sci.* **2016**, *6*, 50. [CrossRef]
40. Lloyd-Hughes, J.; Jeon, T.-I. A review of the terahertz conductivity of bulk and nano-materials. *J. Infrared Millim. Terahertz Waves* **2012**, *33*, 871–925. [CrossRef]
41. Richter, C.; Schmuttenmaer, C.A. Exciton-like trap states limit electron mobility in TiO_2 nanotubes. *Nat. Nanotechnol.* **2010**, *5*, 769–772. [CrossRef]
42. Chen, G.; Shrestha, R.; Amori, A.; Staniszewski, Z.; Jukna, A.; Korliov, A.; Richter, C.; Fray, M.E.; Krauss, T.; Sobolewski, R. Terahertz time-domain spectroscopy characterization of carbon nanostructures embedded in polymer. *J. Phys. Conf. Ser.* **2017**, *906*, 012002. [CrossRef]
43. Dadrasnia, E.; Lamela, H.; Kuppam, M.B.; Garet, F.; Coutza, J.-L. Determination of the DC electrical conductivity of multiwalled carbon nanotube films and graphene layers from noncontact time-domain terahertz measurements. *Adv. Condens. Matter Phys.* **2014**, *2014*, 370619. [CrossRef]

© 2019 by the authors. Licensee MDPI, Basel, Switzerland. This article is an open access article distributed under the terms and conditions of the Creative Commons Attribution (CC BY) license (http://creativecommons.org/licenses/by/4.0/).